ELSEVIER SAUNDERS

NEUROIMAGING CLINICS OF NORTH AMERICA

Neuroimag Clin N Am 16 (2006) 269–283

MR Spectroscopy and Spectroscopic Imaging: Comparing 3.0 T versus 1.5 T

Ulrike Dydak, PhD[a,*], Michael Schär, PhD[b,c]

Proton (^{1}H) MR spectroscopy reveals several neurochemical compounds in vivo and thus is suited for the study of biochemical processes in physiology and in disease. The noninvasive nature of this technique makes it an ideal diagnostic tool in a large variety of diseases including brain tumors, metabolic disorders such as adrenoleukodystrophy and Canavan's disease, Alzheimer's disease, hypoxia secondary to trauma or ischemia, HIV dementia and lesions, and systemic disease such as hepatic and renal failure [1].

The main metabolites analyzed in ^{1}H MR spectroscopy of the brain are N-acetylaspartate (NAA), choline-containing compounds (Cho), creatine and phosphocreatine (Cr), glutamate/glutamine (Glx), myo-inositol (mI), lactate (Lac), and lipids (Lip). NAA is found only in neurons, and is reduced in many brain disorders (eg, infarcts, brain tumors, epilepsy, multiple sclerosis, and neurodegenerative diseases), while it is increased in Canavan's disease. Cho signal is generated by glycerophosphocholine, phosphocholine, and free choline, which participate in membrane synthesis and degradation. Cho is increased in demyelinating diseases and in brain tumors, while it is reduced in hypomyelinating diseases. Cr indirectly reflects energy metabolism and often is used as a reference peak to normalize metabolite signal intensities, as its signal is relatively constant under various pathological processes. With glutamate being an excitatory neurotransmitter and glutamine a substrate for glutathione and glutamate, Glx peaks play an important role in the study of neurotransmission. Glx peaks are known to increase in neurodegenerative diseases, epilepsy, hepatic encephalopathy, and ischemia. mI is considered a glial marker, and it is increased in demyelinating diseases and in dementia. Lac is often not detectable in normal conditions because of its low concentration, but it is increased when energy metabolism is deranged (ischemia, brain tumors, mitochondrial disturbances). The possibility to assess metabolites playing vital roles in neurotransmission, such as γ-aminobutyric acid (GABA), and in neurodegeneration, such as glutathione (GSH), also raises interest in MR spectroscopy for psychiatric applications. A recent review of brain metabo-

This article was written through equal contribution by both authors.
[a] Institute for Biomedical Engineering, University and ETH Zurich, CH-8092 Zurich, Switzerland
[b] Division of MR Research, Department of Radiology, Johns Hopkins University, JHOC Room 4243, 601 North Caroline Street, Baltimore, MD 21287, USA
[c] Philips Medical Systems, Inc., 595 Miner Road, Cleveland, OH 44143, USA
* Corresponding author.
E-mail address: ulrike.dydak@ethz.ch (U. Dydak).

1052-5149/06/$ – see front matter
doi:10.1016/j.nic.2006.02.002
neuroimaging.theclinics.com

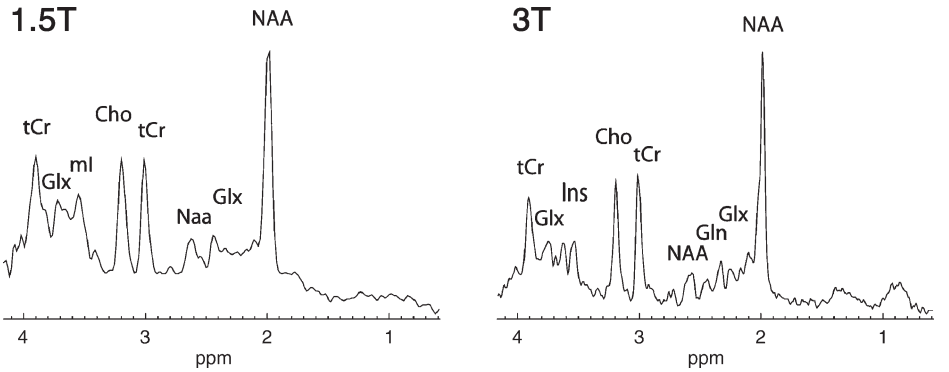

Fig. 1. ^{1}H spectrum (TE = 31 milliseconds) from a volume of interest placed in parietal white matter (40 × 15 × 20 mm^3) acquired at 1.5 T and at 3.0 T in the same healthy volunteer (TR = 2000 milliseconds, 128 averages). Linear shimming was applied at 1.5 T, while second order shimming was used at 3.0 T.

lites with their MR spectroscopy properties and biochemical significance can be found in a paper by Govindaraju and colleagues [2].

In MR spectroscopy, each metabolite is localized on a horizontal frequency scale, called chemical shift [Fig. 1]. Their relative concentration is determined from the area underneath each metabolite's peak. Spectral quality of in vivo MR spectroscopy is not sufficient to separate the nearly 20 metabolites contributing to the spectrum because of overlapping of resonance lines, caused by a small chemical shift range together with broad peaks. The splitting of resonance lines into complex multiple structures further complicates the interpretation of spectra. Therefore, many MR spectroscopy studies with low-field (no more than 1.5 T) MR systems observe only the predominant singlet peaks of NAA, Cr, and Cho, while the information of all the other metabolites contained in the spectrum often is neglected. The signal assignment to metabolites significantly improves when measuring at the highest static magnetic field strengths (B_0) available [3].

The immense commercial success of MR scanners with a B_0 of 3.0 T over the last few years has been driven mostly by advantages given in functional MR imaging and angiography of the brain [4,5]. Also MR spectroscopy has been declared to profit vigorously by an increased B_0: the theoretically predicted linear increase in signal-to-noise ratio (SNR) and in spectral resolution with increasing B_0 [6,7] has been used successfully as a selling point with the potential to reduce long scan times or improve spectral and spatial resolution, and therefore improve quantification. Most published studies directly comparing the performance of ^{1}H MR spectroscopy at 3.0 T and at 1.5 T, however, reported an increase in SNR and spectral resolution much smaller than a factor of two [8–11]. Challenges of ^{1}H MR spectroscopy at higher field strengths, such as shorter transverse (T2) and longer longitudinal relaxation times (T1) of metabolites, increased susceptibility effects, larger chemical shift displacements, and excitation radio frequency (RF) field (B_1) inhomogeneities, explain where the promised gain is lost. A short review about the importance of each effect is given in the following section.

Physical background

A short physical excursion is necessary to understand what happens if B_0 is increased. Table 1 summarizes the main parameters that depend on B_0. The exact physics may be looked up in a textbook [12–14]. The summary in Table 1 is oversimplified, as the different parameters may depend on each other and on further parameters. For example, SNR depends not only on the induced voltages in the coils, but also on B_1-sensitivity of the transmit/receive coils and on the relaxation of the magnetization (T1/T2). All these B_0-dependent changes translate into potentials and drawbacks in MR spectroscopy.

The main assets are the increase in SNR and chemical shift. The increased SNR may be traded according to the magic MR triangle

$$SNR \propto voxel\ size \cdot \sqrt{acquisition\ time} \qquad (1)$$

to decrease voxel size or acquisition time. The factor of two in chemical shift at 3.0 T relative to 1.5 T translates directly into a doubled spectral separation that improves peak conspicuity/resolution and quantification.

Signal-to-noise ratio versus T1, T2, and T2*

The omnipresent factor of two in SNR when increasing B_0 from 1.5 T to 3.0 T comes from the fact

Table 1: Overview of B_0-dependent parameters in magnetic resonance spectroscopy

Signal/noise	~B_0	$U_{Signal} \propto -M_0\, 2\pi\upsilon_0 \cos 2\pi\upsilon_0 t$ $U_{Noise} = \sqrt{4k_bT\,(R_{patient} + R_{coil})\,\Delta f}$	Electromotive force Johnson-Nyquist noise
Chemical shift	~B_0	$B_{shielded} = B_0(1-\sigma)$	Structural factors change B_0 experienced by nucleus
Relaxation times	T1~$\sqrt[3]{B_0}$, T2 ↘		Differs locally and for different metabolites
B_0 inhomogeneity	~B_0	$\Delta B_0 = \chi B_0 \Rightarrow \frac{1}{T2^*} = \frac{1}{T2} + \gamma\,\Delta B_0$	Local field depends on tissue susceptibility
B_1 inhomogeneity	increases		Depends on bodysize and wavelength
Specific absorption rate	~B_0^2	$SAR \propto W \propto \tau\upsilon_0^2 B_1^2 = \frac{B_0^2\alpha^2}{\tau}$	Deposited energy

B_0 denotes the static magnetic field strength; U, the induced voltage; M_0, the transverse magnetization; ν_0, the Larmor frequency; k_b, the Boltzmann constant; T, the absolute temperature of the resistive object; R, the resistance induced by patient or coil; Δf, the receiver bandwidth, σ the chemical shift; T1, the longitudinal and T2 the transversal relaxation times; χ, the tissue susceptibility; T2*, the transversal relaxation time incorporating the transversal magnetization loss due to B_0 field inhomogeneity; γ, the gyromagnetic ratio of the nucleus under investigation; B_1, the radio frequency field; W, the work; τ, the excitation pulse duration; and α, the flip angle [12–14].

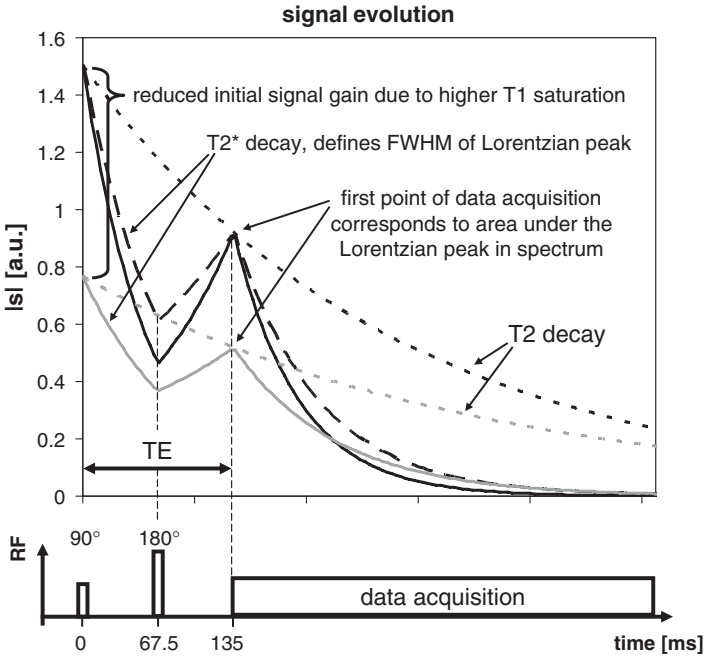

Fig. 2. Evolution of the absolute value of the signal in a spin echo experiment as calculated with parameters for NAA from the literature. Black lines are calculated with parameters corresponding to a B_0 of 3.0 T, while gray lines correspond to 1.5 T. The dotted lines show the signal decay caused by T2 decay, the solid line the decay caused by T2* when using linear shimming, and the dashed line the decay caused by T2* when using second order shimming at 3.0 T. The ratio of the initial signal after the 90° excitation pulse between 3.0 T and 1.5 T is slightly less than a factor of two because of increased T1 saturation at 3.0 T. The area under the Lorentzian peak after fast Fourier transform [Fig. 3] is given by the signal amplitude of the first point of the data acquisition at the echo top, and therefore depends on the echo time TE and T2. The following tissue and sequence parameters were used (3.0 T/1.5 T): TR = 2 seconds, TE = 135 milliseconds, T1 = 1411 milliseconds/1357 milliseconds [17,18], T2 = 276 milliseconds/345 milliseconds [18], T2* = 72 milliseconds/125 milliseconds when using linear shimming, and T2* = 103 milliseconds at 3.0 T with second order shimming.

that the induced voltage in the receive coils goes with the square of B_0, while the Johnson-Nyquist noise increases linearly with B_0. The actual signal acquired in an MR measurement, however, is given by the steady state of the magnetization, which depends on tissue parameters T1 and T2 and on sequence parameters such as repetition time (TR) and echo time (TE). Most of these parameters depend on B_0 also.

The T1 and T2 behavior of free water at different field strengths has been reported by Bottomley and colleagues [15] and is shown in Table 1. T1 values increase, and T2 values decrease with increasing magnetic field strength. First published T1 and T2 values of normal brain metabolites at 3.0 T [8,16–18] have shown that the increase in T1 is only minor and that T2 decreases significantly. T1 and T2 values of brain metabolites show regional variations at 3.0 T, which can be attributed to differences in relative white matter to gray matter contents [17,18].

The signal evolution for a spin echo sequence is shown in Fig. 2. For in vivo MR spectroscopy localization in the brain, usually a double spin echo such as point-resolved spectroscopy (PRESS [19]) or a stimulated echo acquisition mode (STEAM [20]) sequence is applied. To understand the relaxation effects at 3.0 T, a single echo sequence is sufficient and easier to understand. T1 and T2 tissue parameters of NAA from the literature, which were measured with the same sequences and in the same brain regions for both field strengths, were chosen and then averaged (T1 = 1411 ms/1357 ms [17,18] and T2 = 276 ms/345 ms [18] at 3.0 T/1.5 T).

Incorporating a fourfold signal and doubled noise, the available SNR at 3.0 T is twice as high as at 1.5 T if magnetization is relaxed fully. As long as the chosen TR is shorter than 5 × T1, the initial signal amplitude after a 90° excitation pulse is reduced, because the time for relaxation is too short for the longitudinal magnetization to reach its equilibrium (T1 saturation). The small increase in T1 when going from 1.5 T to 3.0 T leads to a minor increase of T1 saturation at the higher field for the NAA metabolite peak.

Magnetic field inhomogeneities lead to a distribution of Larmor frequencies in macroscopic tissue volumes, which leads to a more rapid loss of transverse magnetization than is caused by pure T2 relaxation. This so-called T2* loss can be recovered with a spin echo sequence [Fig. 2] [21]. Therefore, the signal amplitude at the start of the data acquisition is given by T2 and the chosen echo time TE of the localization sequence.

The Fourier transform of an exponentially decaying signal gives a Lorentzian peak [Fig. 3], where the area under the peak is equal to the amplitude

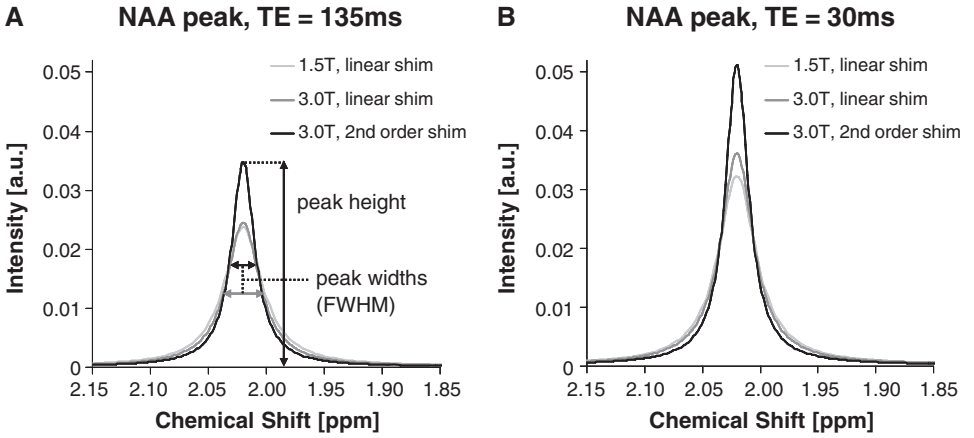

Fig. 3. The fast Fourier transformed (FFT) data of the simulated NAA signal in Fig. 2 at an echo time TE of 135 milliseconds (*A*) and 30 milliseconds (*B*) for a field strength B_0 of 1.5 T (*light gray*) and 3.0 T with linear (*gray*) and second order shimming (*black*). The FFT of exponentially decaying data lead to Lorentzian-shaped peaks. The area under a peak is given by the signal amplitude of the first point of the data acquisition [Fig. 2], and therefore is the same for the two peaks simulated at 3.0 T with linear and second order shimming. The peak width or the full width at half maximum (FWHM) of a Lorentzian peak is given by $1/(\pi\ T2^*)$. When incorporating the changes in T1, T2, and T2* the peak height (not area under peak) increases only by 3% (11%) at a TE of 135 milliseconds (30 milliseconds) when increasing B_0 from 1.5 T to 3.0 T. This can be improved to 46% (58%) by using second order shimming. The following tissue parameters were used (3.0 T/1.5 T): TR = 2 seconds, TE = 135 milliseconds, T1 = 1411 milliseconds/1357 milliseconds [17,18], T2 = 276 milliseconds/345 milliseconds [18], T2* = 72 milliseconds/125 milliseconds when using linear shimming and T2* = 103 milliseconds at 3.0 T with second order shimming.

of the first data point of the signal acquisition, and therefore depends on TE and T2, but not on T2*. Because of T2 shortening at higher fields, the initially doubled SNR at 3.0 T shrinks to a factor 1.78 at a TE of 135 milliseconds. This factor can be improved to 1.92 when the echo time is reduced to 30 milliseconds, but it will be worse at longer echo times.

During data acquisition, signal decays with T2*. The shorter T2* is, the faster the signal decays. Although the area under the peak is independent of T2*, the peak height will decrease, and the peak becomes broader when T2* gets shorter. At 3.0 T, T2* is significantly shorter than at 1.5 T [formula in Table 1]. Hence, spectral peaks are broader at 3.0 T than at 1.5 T, and the improved spectral separation is nearly lost. When comparing peak heights, the ratio between the two field strengths drops from the initial 2.00 to 1.03 and 1.11 for TEs of 135 and 30 milliseconds, respectively.

Second order shimming

By applying second order shimming instead of linear shimming, the field homogeneity in the brain has been shown to be improved by about 40% [22]. Clinical 3.0 T scanners usually are equipped with higher order shimming capabilities, which is seldom the case for 1.5 T scanners. A 40% improvement in field homogeneity in the NAA example increases T2* and reduces the peak width. The peak height grows accordingly, and the peak height ratio between the field strengths improves to 1.46 and 1.58 at a TE of 135 and 30 milliseconds, respectively [Fig. 3]. Although higher order shimming remains a challenge in some body parts, second order shimming is a clear must in the brain where automatic shim algorithms like FASTMAP (fast, automatic shimming technique by mapping along projections) [23] perform robustly and fast.

From these considerations, it follows that spectral quantification has to be done with fitting routines measuring the area under the peaks rather than peak heights. The most widely used, commercially available fitting routine is the linear combination of model spectra (LCModel) [24]. The model spectra are acquired from metabolite solutions in vitro. LCModel is fully automatic, which makes the method more objective compared with fitting routines that require user interaction.

The shorter T2 at the higher B_0 seems to eat away half of the expected gain. However, it also leads to a flatter baseline in the region between NAA and Cr peaks when using long TEs [Fig. 4]. While it reduces all peaks, it leads to a total disappearance of the broader peaks, such as Glx, macromolecules, and lipids. The flatter baseline contributes to more precise quantification of the main three singlet peaks NAA, Cr, and Cho in MR spectroscopic imaging at a TE of 144 milliseconds.

Another promising approach to reduce the line width of metabolite peaks in MR spectroscopic imaging is to use smaller voxel sizes. It has been shown that the line width drops quickly in MR spectroscopic imaging voxels no more than 0.4 cm^3, most probably reflecting a sudden increase in homogeneity caused by the fact that less heterogeneous tissue is being sampled [25].

Spectral resolution

Doubling the field strength doubles the resonance frequency, and therefore the distance between the metabolite peaks. As discussed in the NAA example of Figs. 2 and 3, this increase in spectral resolution is lost partly because of decreasing T2 and T2* values. The NAA example shows that the initial 100% increase in spectral resolution is decreased to 22% with linear shimming. Second order shimming restores an increase of 73%.

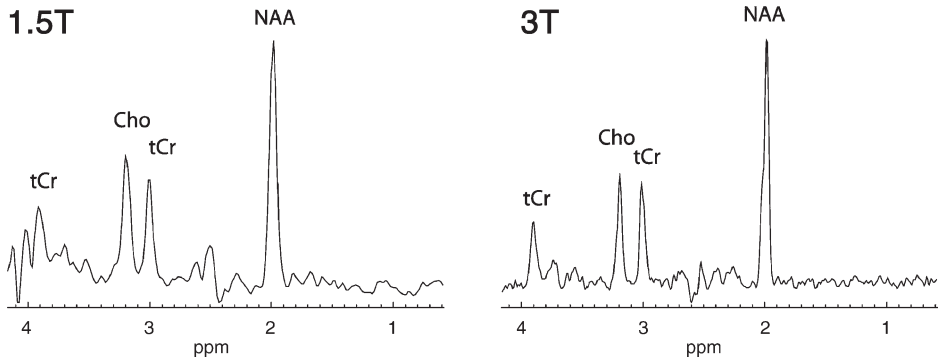

Fig. 4. ^{1}H spectrum (TE = 144 milliseconds) from a volume of interest placed in parietal white matter (40 × 15 × 20 mm^3) acquired at 1.5 T and at 3.0 T in the same healthy volunteer (TR = 2000 milliseconds, 128 averages). Linear shimming was applied at 1.5 T, while second order shimming was used at 3.0 T.

So far most studies on 3.0 T MR spectroscopy have been performed with linear shimming only. This might explain some of the not so enthusiastic results presented at the higher field strength. Nevertheless, the increased spectral resolution at 3.0 T has been reported to allow for quantification of Glx [10] and mI [11], which are difficult to quantify at 1.5 T because of significant spectral overlap of strongly coupled spin systems.

An alternative approach to the straight-forward data fitting is the use of acquisition-based methods. The goal of these methods is to simplify the crowded spectrum, and, therefore, make quantification easier and more reliable. Such a simplification may be achieved in two ways. In the first approach, the spectral information is reduced to selectively acquire only the desired signal, (eg, of one single metabolite). These so-called spectral editing techniques [26,27] have a low inherent sensitivity and will profit from the increased available SNR at higher field strengths. In the second approach, using so-called two-dimensional acquisition schemes, the entire signal information is spread out into multiple spectral dimensions by additional encoding of the signal [26,28]. Improved spectral dispersion at 3.0 T enables these sequence types to better quantify the coupled resonances of GSH [29], Glx, and mI [30–32]. Two-dimensional MR spectroscopy sequences have very high potential for localized single-volume studies at high field. The full clinical realization of this potential, however, has yet to be achieved.

B_1 inhomogeneity and specific absorption rate

Further sources of signal loss are inhomogeneous or wrongly calibrated excitation RF fields B_1. In case B_1 has not the intended amplitude in the tissue of interest, the excitation and refocusing pulses become less efficient, as not all magnetization is excited or refocused [Fig. 5]. Although B_1 remains homogeneous in the head at 3.0 T (plus or minus 10%) when using a dedicated head coil, huge variations may arise in phantoms. This has to be considered when phantom measurements are used for absolute quantification.

Power deposition and specific absorption rate (SAR) limitations are usually not an issue in spectroscopic acquisitions, as the repetition times are much longer compared to MR imaging. MR spectroscopy examinations, however, usually are performed in conjunction with MR imaging, using the same coils. Most transmit coils used for imaging have limited B_1 amplitudes, which at 3.0 T is half the value used at 1.5 T to stay within the safety regulations. This leads to a doubling of the excitation pulse duration and therefore pulses with only half the bandwidth. The impact of these changes on MR spectroscopy is discussed in the section on localization.

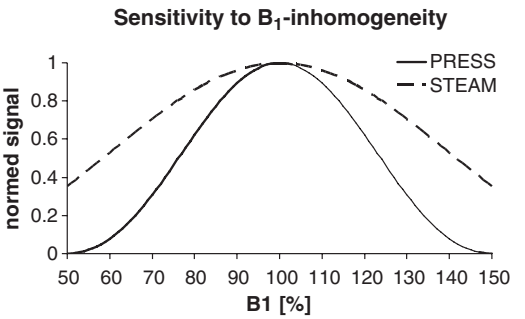

Fig. 5. Sensitivity of the acquired signal to B_1-inhomogeneity for PRESS (*solid line*) and STEAM (*dashed*) localization methods. B_1-inhomogeneities experienced in the brain at 3.0 T (plus or minus 10%) do not pose a problem. B_1-inhomogeneities and resulting signal loss in certain phantom containers, however, may be significant.

Scan time

One of the major user complaints for brain spectroscopic imaging at 1.5 T is the lengthy scan time required for high resolution or for three-dimensional scans. In fact, many of the exciting opportunities for MR spectroscopic imaging (MRSI) demand extended anatomic coverage while maintaining a good spatial resolution (eg, predicting sites of tumor recurrence). Furthermore, it has been demonstrated that using high resolution in MRSI at 3.0 T has the important advantage of a less than linear loss in SNR with decreasing voxel size (ranging between 44% and 60% for resolutions from 0.75 cm^3 to 0.094 cm^3) because of the decreasing line width [25]. On the other hand, many patients cannot tolerate extended (perhaps 30-minute) scans commonly appended to routine clinical MR imaging. Furthermore, with the present status of MR spectroscopy in the United States as a nonreimbursable procedure, extended scan times are prohibited, and consequently potential applications of the technology are not revealed.

Compared with MR imaging, MRSI has an additional chemical shift dimension to be sampled for every point in spatial k-space. To have adequate spectral resolution, the sampling time of this dimension needs to be at least several hundred milliseconds (the spectral resolution is the inverse of the sampling time), which makes MRSI inherently much slower than MRSI. In the past, many fast MR spectroscopic techniques have been proposed, ranging from k-space weighting by varying the

repetition time [33], to multiple spin echo MRSI [34], and fast sequences based on various fast-imaging sequences such as FLASH [35], fast gradient echoes [36], EPI [37, 38], U-FLARE [39], BURST [40], GRASE [41], or spiral imaging [42]. At 1.5 T, such techniques have achieved scan times of only 21 minutes for the acquisition of 32 × 32 × 12 MRSI voxels (volumetric multi-shot echo–planar spectroscopic imaging [43]) or 17 minutes for a 36 × 36 × 32 voxel matrix (three-dimensional variable-density spiral chemical shift imaging [44]) for volumetric human brain MRSI. Frequently, the reduction in scan time is achieved at the expense of parameter restrictions, such as reduced spectral resolution or bandwidth. Furthermore, many of these fast techniques require long multiple (gradient or spin) echo trains, which become more problematic at 3.0 T because of the reduced T_2 and T_2* at high field strength, or because of restrictions of power deposition (multiple refocusing pulses). The fastest sequences, based on echo–planar or spiral imaging, are very sensitive to timing inaccuracies, eddy currents, concomitant gradient effects, and B_0 field inhomogeneities. Presently, the only publication found on using either of these two techniques applied to human body MRSI at field strengths above 1.5 T is a paper on multi-voxel two-dimensional J-resolved spiral chemical shift imaging of the prostate at 3.0 T [45]. Recently, new work has been presented at conferences with promising results of proton echo–planar spectroscopic imaging (PEPSI) and spiral spectroscopic imaging of the human brain at 3.0 T and even 4.0 T [46–49]. Using flyback echo–planar encoding, high spectral resolution three-dimensional MRSI of cancer in the human brain (16 × 16 × 16 voxels) has been shown to be achieved in only 8.5 minutes at 3.0 T [50].

A recent advance in MR imaging—parallel imaging with sensitivity encoding (SENSE) [51]—has allowed scan time reduction for many MR sequences. SENSE also has proven to be a perfect match for high-field imaging because of multiple other benefits, such as allowing the reduction of echo train lengths in multi-echo sequences with commensurate improvement in image quality [52]. In SENSE, the number of phase-encoding steps is reduced by the SENSE reduction or acceleration factor. The spatial information is recovered in the reconstruction by relying on post processing of signals from multiple receiver coils. In three-dimensional MR imaging, there are two phase-encoding dimensions, allowing acceleration factors to multiply (it is now common to see doubly accelerated three-dimensional MR imaging scans). In fact, conventional MRSI represents an even more attractive opportunity for parallel acquisition. Even two-dimensional MRSI uses two phase-encoding dimensions (there is no readout gradient) and thus potentially is accelerated doubly. SENSE-MRSI [53], with a SENSE reduction factor of two in both spatial dimensions, has been shown to increase the speed of MRSI by a factor of four, while maintaining spatial and spectral resolution and losing only the obligatory factor of $\sqrt{4} = 2$ in SNR. This loss in SNR can be critical in some applications at 1.5 T. The signal boost at 3.0 T, however, may be used to alleviate SNR losses because of the fourfold acceleration. Furthermore, SENSE may be combined with other fast MRSI

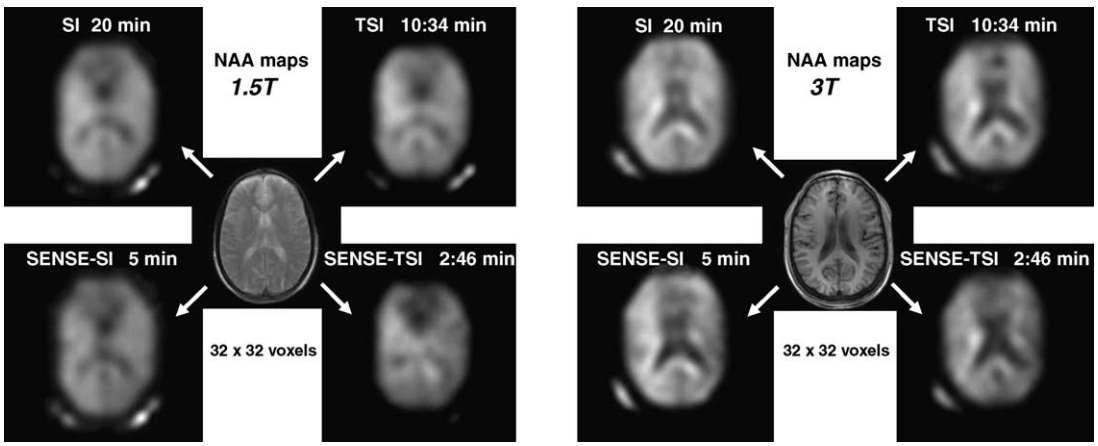

Fig. 6. NAA maps from high-resolution MRSI scans (32 × 32 matrix over a field of view of 230 mm, spectral resolution = 1.5 Hz at 1.5 T, 2 Hz at 3.0 T) acquired with conventional MRSI in 20 minutes, with SENSE (factor 2 × 2) in 5 minutes, with multi-spin echo MRSI (TSI) in 10:34 minutes and SENSE-TSI in 2:46 minutes at both field strengths 1.5 T and 3.0 T in two different healthy volunteers. The loss in SNR is observable in the SENSE-TSI metabolite map at 1.5 T as ventricles are not outlined clearly. At 3.0 T, however, the SNR is high enough to generate high-quality NAA metabolite maps even in the fastest acquisition.

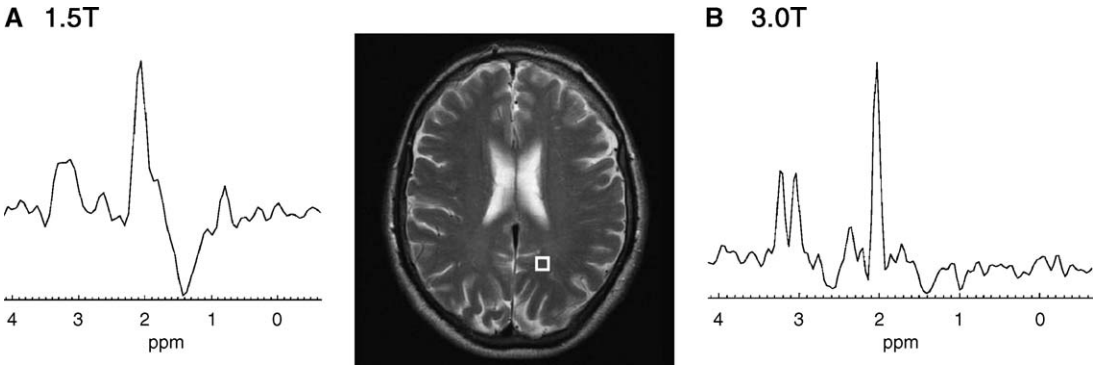

Fig. 7. Example spectra from a multi-spin echo MRSI (TSI) scan with an interecho spacing of 144 milliseconds acquired once at (*A*) 1.5 T (Δf = 8 Hz) and once at (*B*) 3.0 T (Δf = 8.8 Hz) in the same healthy brain. Although a spectral resolution of 8 Hz is not sufficient to resolve Cho and Cr at 1.5 T, it is at 3.0 T.

techniques making use of phase encoding (eg, with PEPSI [54] or multiple spin echo MRSI, called turbo spectroscopic imaging [TSI]). The latter also uses two phase-encoding dimensions for two-dimensional MRSI and therefore readily profits from high SENSE acceleration factors. Combined, SENSE and TSI [Fig. 6] have been shown to allow for accelerations of up to a factor of nine for in vivo applications [55].

At 3.0 T, the TSI sequence offers the possibility of trading the higher spectral resolution against better SNR or speed, which is not possible at 1.5 T. Because a certain spectral resolution requires a minimum acquisition time for each spin echo, the interecho spacing needs to be sufficiently long. This in turn limits the total echo train length. As an example, the echo sampling time needs to be at least 200 milliseconds to obtain a 5 Hz nominal spectral resolution necessary to distinguish Cr from Cho at 1.5 T, which usually restricts the total echo train length to four. At 3.0 T, however, because of the higher spectral dispersion, a 10 Hz nominal spectral resolution is sufficient to separate Cr from Cho [Fig. 7]. Therefore a sampling time of only 100 milliseconds becomes feasible, allowing shorter interecho spacing, while keeping the same spectral resolution on the ppm scale as at 1.5 T with a sampling time of 200 milliseconds.

As the shorter echo sampling time allows each spin echo in the TSI sequence to be sampled at an earlier time (eg, after 100 milliseconds, 200 milliseconds, 300 milliseconds, …. instead of after 200 milliseconds, 400 milliseconds, 600 milliseconds, …), the echo signals have endured less T2 loss and thus the gain in SNR at 3.0 T is much higher than resulting from the higher field strength alone. Fig. 8 shows an example at 3.0 T, where a factor of two was gained in signal, simply by reducing the sampling time (=trading the extra spectral dispersion at 3.0 T against SNR).

The shorter echo sampling times also enable longer total echo train lengths and thus a significant reduction in total scan time. Knowing T2, it can be calculated that the sixth spin echo at 3.0 T (using an interecho spacing of 144 milliseconds) has suffered about as much T2 loss as the fourth spin echo at 1.5 T (using an interecho spacing of 288 milliseconds to obtain the same spectral reso-

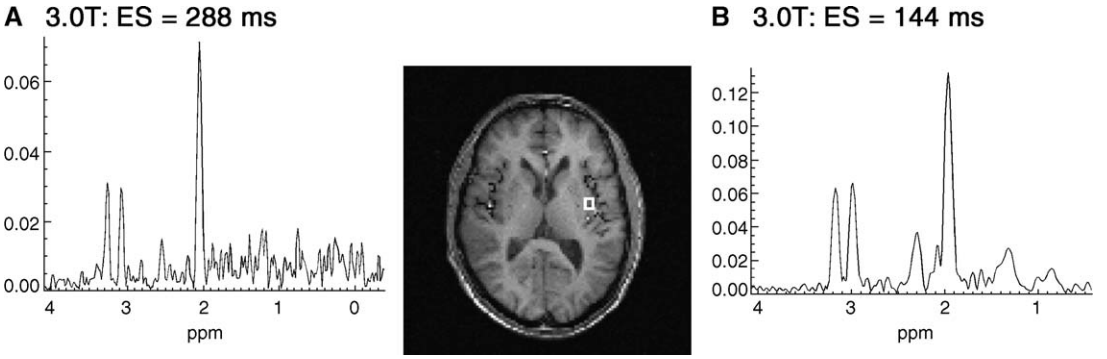

Fig. 8. Example spectra from a multi-spin echo MRSI (TSI) scan acquired at 3.0 T from the same healthy volunteer (*A*) with an interecho spacing (ES) of 288 milliseconds and (*B*) with an ES of 144 milliseconds, trading the spectral resolution against SNR.

lution). As TSI with an echo train length of four has given good results in clinical MR spectroscopic studies at 1.5 T [56–60], TSI with an echo train length of six (TSI6) should be a sensible choice for 3.0 T. First results of TSI with long echo train length and with high spatial resolution are promising [Fig. 9]. Furthermore, the combination of SENSE, TSI, and long echo train length results in yet another significant reduction of scan time. Single-slice MRSI of the human brain with a 24 × 24 matrix becomes possible in only 54 seconds [Fig. 10], and the acquisition of six slices with 20 × 20 voxels each only takes 3.18 minutes [61]. The point spread function, and therefore also the discrepancy between real and nominal spatial resolution of TSI scans, worsens with longer echo train length.

Three-dimensional MRSI, with three dimensions of phase encoding, offers the possibility of cubic acceleration using SENSE. As SENSE acceleration in all three spatial dimensions requires specially designed coil arrays and at least eight acquisition channels, MRSI with simultaneous SENSE reduction in all three dimensions is currently work in progress. Already, however, doubly accel-

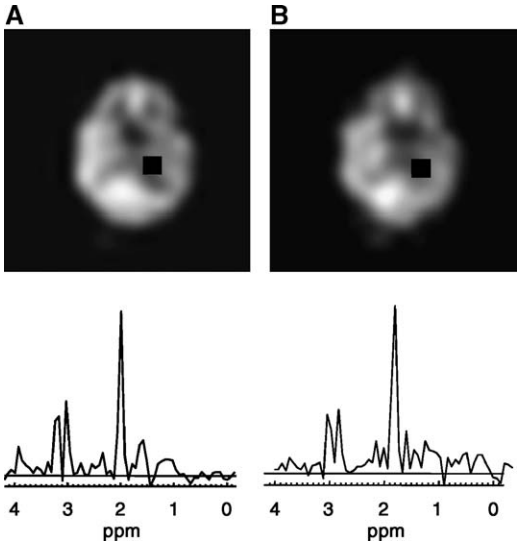

Fig. 10. Combination of SENSE and TSI (six spin echoes) at 3.0 T. Choline maps and example spectrum from a 24 × 24 matrix MRSI scan in a healthy brain acquired (*A*) with conventional MRSI in 11:23 minutes and (*B*) SENSE-TSI (SENSE factor 4, TSI factor 6) in 54 seconds.

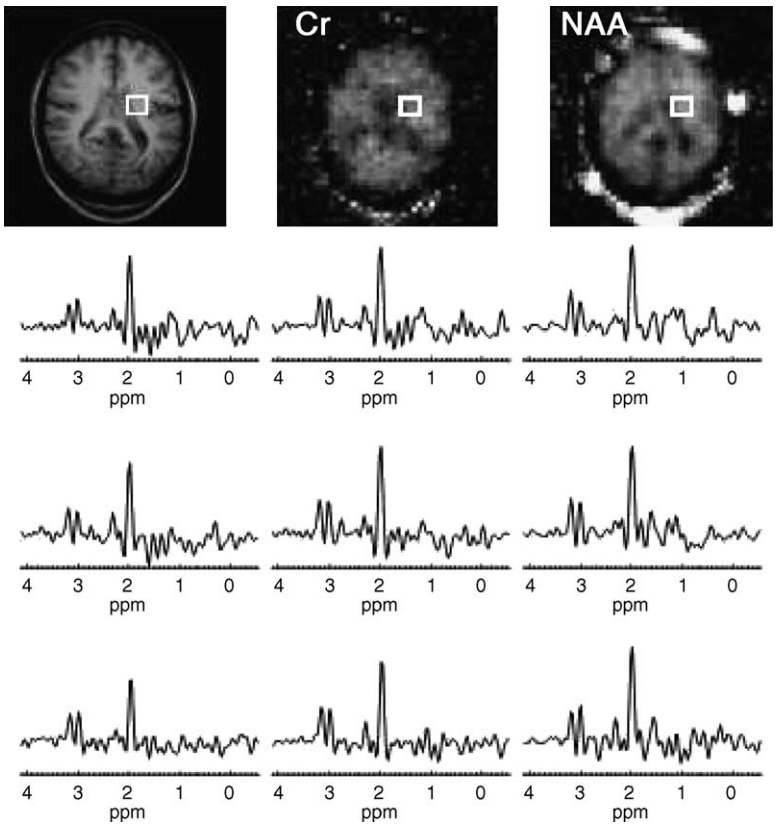

Fig. 9. Multi-spin echo MRSI (TSI) scan with an echo train length of nine (TE = ES = 144 milliseconds, 40 × 40 voxels, nominal spatial resolution = 0.375 mL) acquired at 3.0 T in only 5 minutes in a healthy volunteer. The metabolite maps are not interpolated and show the high spatial resolution of this scan.

erated SENSE reduces impossible scan times of three-dimensional MRSI (approximately 1 hour) down to acceptable scan times of 14 minutes (eg, for the acquisition of 24 × 24 × 6 voxels) [Fig. 11]. As has been shown in a study on spatial resolution in MRSI performed on a human brain tumor [62], pathological changes may occur only in a small fraction of the volume of interest. With low spatial resolution, these changes may be masked or even completely obscured by partial volume effects. The same argument holds true for all three dimensions, as tumors and other brain lesions usually do not fit into a single slice or a rectangular box. Fig. 11 shows an example where Lac/Lip signal and the signals from NAA, Cho, and Cr change rapidly (over a few millimeters) not only within one slice, but also throughout the slices. In a conventional single-slice MRSI setup with a slice thickness of 1.5 to 2 cm, these different spectra would not be differentiated because of partial volume effects.

As has been discussed previously, the higher field strength not only brings advantages, but also some challenges. This can also be seen in three-dimensional MRSI applications, where scan time is one of the most stringent limitations, but not the only one. Achieving a good homogeneity over a large region of the brain, including lesions, edema, cerebrospinal fluid and healthy brain tissue is not always easy and becomes more difficult at 3.0 T. This in turn can lead to problems obtaining good water suppression over the whole brain. Another problem is the suppression of subcutaneous fat over the whole skull for all different patient head geometries, while being able to obtain signal from brain regions close to the skull. Higher order shimming and improved outer volume or fat suppression pulses will be necessary for such applications at 3.0 T.

Further progress in the different techniques of fast MRSI, such as EPI-, spiral-, and SENSE-based sequences at high field strength, and possibly even their combination, are still required, but there is no doubt that they hold great promise for investigating the whole brain metabolism in all three dimensions with high spatial resolution in patient-friendly scan times.

Localization: chemical shift misregistration

The exact origin of the spectral signal is an important issue in MR spectroscopy, whether one is looking at the metabolic signal in small anatomical regions (eg, the hippocampus), or at healthy looking tissue close to a tumor border. When prescribing a volume of interest for the MR spectroscopy measurement on an MR image, however, the shown box delineates the signal origin of exactly one resonance frequency. On most scanners, this frequency is set to the frequency of NAA at 2.02 ppm. For all other frequencies, the signal origin is shifted spatially. The amount of shift depends on the chemical shift of the metabolite and on the bandwidth of the applied RF pulses, as it is this bandwidth, together with the strength of the encoding gradients that defines the volume of spin excitation for a given frequency. The fact that each peak comes from a slightly different volume is true for all field strengths, but if the shift is small enough, it usually is ignored. This is mostly the case at

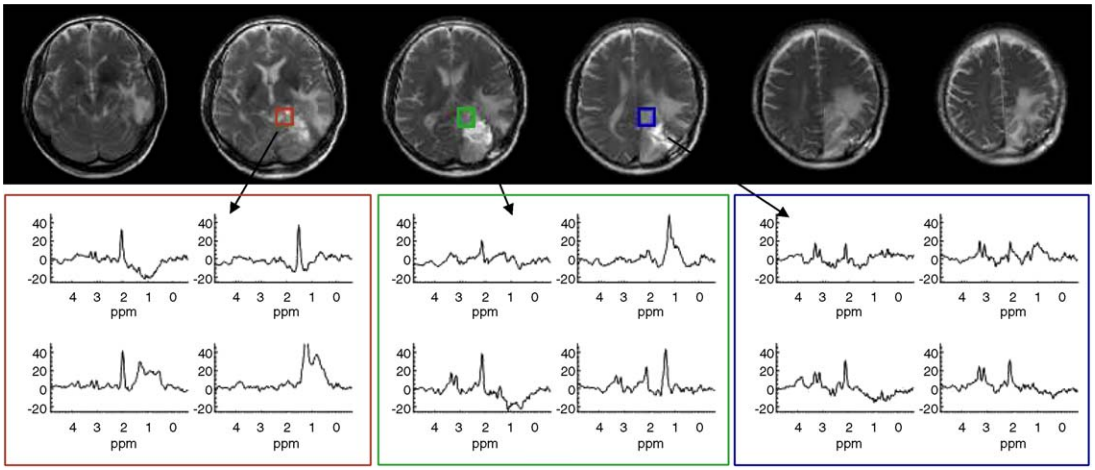

Fig. 11. Three-dimensional SENSE-MRSI acquisition at 3.0 T (24 × 24 × 6 voxels, nominal spatial resolution 0.8 cm^3, spectral resolution 1.5 Hz; 2 × 2 voxels from three adjacent slices are displayed, showing how metabolism changes within millimeters in all three dimensions (note the changes in the right lower spectrum over the three slices).

1.5 T, although even there care should be taken when comparing metabolite ratios from voxels on one border with voxels on the other border of a chosen volume of interest in a spectroscopic imaging examination.

To calculate the size of the chemical shift misregistration Δx, one needs to know the chemical shift Δω between the reference metabolite (NAA) and the metabolite of interest and either the excitation volume size l and the bandwidth BW_{pulse} of the slice-selective RF pulse or the strength of the applied gradient G_{slice} during the slice selective pulse:

$$\Delta x = \frac{\Delta\omega \cdot l}{BW_{pulse}} = \frac{2\pi}{\gamma}\frac{\Delta\omega}{G_{slice}}. \quad (2)$$

At higher field strength, the chemical shift difference between the metabolites increases, and at the same time, the bandwidth of most commonly used excitation and refocusing pulses decreases because of safety issues. In combination with the increased chemical shift dispersion, this leads to a significant misregistration problem at 3.0 T, which scales roughly with the square of the field strength. Metabolite peaks resonating at frequencies higher than the NAA-frequency, such as the Cho and Cr resonances, are excited in a volume shifted to one side compared to the selected volume of interest on the localizer image, while metabolite peaks with lower frequencies than NAA, such as the Lac doublet or lipid peaks, stem from a volume shifted to the opposite side [Fig. 12].

The shift of the excitation volume of choline, for example, with respect to the volume on the localizer MR image, which is calculated for NAA, can be up to 20% of the prescribed voxel length in each dimension. The exact amount of shift depends on the allowed B_1 amplitude and therefore on the used coil and vendor. Whereas this problem may be seen clearly in certain spectroscopic imaging experiments [see Fig. 12], it is equally present in single-voxel examinations, where no artifact reminds of its presence. For coupled spin systems (eg, lactate), the chemical shift misregistration may lead to dramatic signal cancellation. A first solution implemented on many clinical MR scanners is to excite the spins in a larger volume, encompassing all shifted volumes of the frequency range of interest, and to use very selective saturation bands to define the intersection of all these volumes, which is the volume depicted on the localizer MR image [63]. Although this is a straight-forward solution for proton spectroscopy at 3.0 T, it is not the way to go for other nuclei such as ^{31}P, or ^{13}C, or for ^{1}H MR spectroscopy at even higher field strengths such as 7.0 T. In these cases, the chemical shift differences increase to such an extent that the excitation volumes for different metabolites might not even overlap in the worst case. Another approach is to use pulses with much larger bandwidths such as adiabatic pulses. Because ordinary adiabatic full passage (AFP) pulses cause a nonlinear phase variation, however, they cannot be used as refocusing pulses. This phase variation can be compensated for by using two AFPs in a double spin echo sequence [64] as applied in LASER (localization by adiabatic selective refocusing) sequences. Pairs of AFP pulses are used for volume selection and echo formation

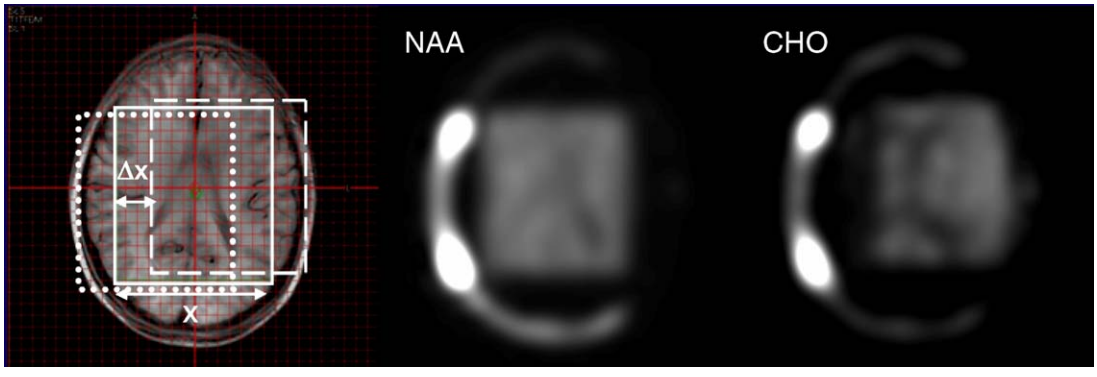

Fig. 12. Artifacts in MRSI at 3.0 T caused by chemical shift misregistration using PRESS localization without outer volume saturation bands. The volume defined by the user on the localizer MR image is depicted as a solid line and defines the volume where NAA is excited. Therefore the NAA image is correct. The Cho is excited in a shifted volume (*dashed line*), however, as can be seen in the choline (CHO) image. The bright artifact on the left in both metabolite images comes from the fact that lipids were excited in a volume shifted to the other side (*dotted line*), covering part of the subcutaneous fat. This leads to a large signal in these areas, which will be misinterpreted as NAA or other metabolites if integration instead of fitting is used to generate metabolite images. The displacement artifact cannot be corrected for in postprocessing, and metabolite images cannot be shifted back as seen from the correct location of the ventricles in the choline image. Voxels in the intersection of all volumes contain the correct amount of each metabolite.

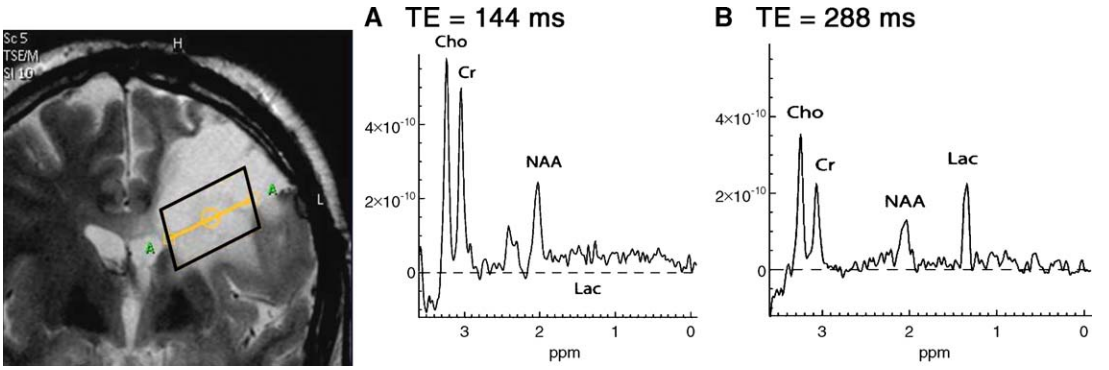

Fig. 13. Clinical example for signal loss caused by chemical shift misregistration. Glioma measured at 3.0 T with single voxel MR spectroscopy, planned as outlined by the black box: (*A*) TE = 144 milliseconds, (*B*) TE = 288 milliseconds. At TE = 144 milliseconds, the lactate signal is not observable, although a clear lactate peak can be seen at TE = 288 milliseconds.

at the same time in all three spatial directions [65,66]. LASER therefore might be a good choice for localization in high-field spectroscopic applications in the future.

J-modulation artifacts: measuring lactate at 3.0 T

The very same problem of chemical shift misregistration at 3.0 T can lead to significant signal loss of coupled spin systems (eg, Lac) at 3.0 T. Lactate is an important marker of anaerobic glycolysis and therefore plays a pivotal role in many brain pathologies such as tumors, stroke, cerebral ischemia, hypoxia, and several mitochondrial disorders [12,67]. An incorrect assessment of the lactate doublet at 1.33 ppm therefore might lead to important errors in diagnosis. In ^{1}H MR spectroscopy, the lactate molecule gives rise to a doublet at 1.33 ppm arising from three magnetically equivalent methyl (CH_3) protons and a quartet at 4.11 ppm arising from the methine protons (CH). This usually is not visible in vivo. These two resonances are coupled weakly, resulting in a phase evolution of the methyl doublet that depends on echo time. For TE = 144 milliseconds, the resonance shows a phase of 180° leading to a negative in-phase doublet, whereas an echo time of 288 milliseconds gives rise to a positive in-phase doublet. Because only in-phase resonances can be quantified, echo times of 144 and 288 milliseconds are preferable for lactate detection and assignment. At 1.5 T, an echo time of 144 milliseconds often is preferred, as the negative lactate doublet is discriminated more easily from lipid signals located at or near the same frequency. The previously described displacement of excitation volumes for different frequencies also affects the two resonances of lactate, giving rise to so-called anomalous J-modulation [68,69]. Only in some part of the defined volume of interest both resonances are excited, and therefore coupling and phase evolution only occurs in that part of the volume. In other parts, the lactate doublet does not evolve at all and stays in phase with the other metabolites. As all signals are added over the whole volume in a single voxel examination, negative and positive signals cancel out at certain echo times, leading to severe underestimation of the total lactate present [Fig. 13]. The amount of signal cancellation can be as high as 80% at TE = 144 milliseconds and depends on pulse bandwidth and allowed maximum B_1 and therefore on used coils and vendor. A good check is to do a phantom measurement. If the negative doublet signal at TE = 144 milliseconds is smaller than the positive doublet signal at TE = 288 milliseconds, which has experienced more T2 decay, then part of the signal at TE = 144 milliseconds has been lost. A detailed explanation of this signal cancellation, including clinical examples and phantom measurements compared over 3.0 T systems from three different vendors can be found elsewhere [70].

Summary

MR spectroscopy is one of the MR techniques that profits from higher magnetic field strength in more than one way. As many applications in MR spectroscopy remain restricted by SNR at 1.5 T, the SNR gain at 3.0 T is more than welcome to enable higher spectral quality, better peak quantification, higher spatial resolution, or fast MRSI. Parallel MRSI (SENSE-MRSI) allows an SNR increase of a factor of two to be transformed into a scan time reduction by a factor of four. The second advantage is the linearly increased spectral separation of the me-

tabolites. The chemical shift in Hz doubles at 3.0 T, enabling better peak separation, quantification, or even peak identification (eg, glutamine/glutamate). This benefit further has implications for minimum echo sampling durations and thus may be traded for SNR or for speed in multi-spin echo MRSI, enabling new fast MRSI techniques.

Many of the benefits, however, are mitigated if parameters, techniques, and sequences are not adapted and optimized for 3.0 T. Although the signal increases quadratically and noise only linearly with the main magnetic field, shorter T2, longer T1, and especially increased field inhomogeneities keep the SNR from doubling and broaden the peak line widths at higher field strength. Higher order shimming is therefore essential if full advantage is to be taken from the increased SNR and spectral dispersion. Furthermore, RF pulses or localization sequences have to be adapted to overcome metabolite misregistration or even signal loss problems.

In summary, once all techniques are clinically available to fully exploit all advantages, 3.0 T may be more than twice as good for MR spectroscopy compared with 1.5 T, promising significant new applications for neuro-MR spectroscopy, such as whole brain MRSI, ultrahigh resolution or dynamic applications.

References

[1] Lin A, Ross BD, Harris K, et al. Efficacy of proton magnetic resonance spectroscopy in neurological diagnosis and neurotherapeutic decision making. NeuroRx 2005;2:197–214.

[2] Govindaraju V, Young K, Maudsley AA. Proton NMR chemical shifts and coupling constants for brain metabolites. NMR Biomed 2000;13: 129–53.

[3] Tkac I, Andersen P, Adriany G, et al. In vivo 1H NMR spectroscopy of the human brain at 7 T. Magn Reson Med 2001;46:451–6.

[4] Krüger G, Kastrup A, Glover GH. Neuroimaging at 1.5 T and 3.0 T: comparison of oxygenation-sensitive magnetic resonance imaging. Magn Reson Med 2001;45:595–604.

[5] Bernstein MA, Huston III J, Lin C, et al. High-resolution intracranial and cervical MRA at 3.0 T: technical considerations and initial experience. Magn Reson Med 2001;46:955–62.

[6] Hetherington HP, Pan JW, Chu WJ, et al. Biological and clinical MRS at ultra-high field. NMR Biomed 1997;10:360–71.

[7] Gruetter R, Weisdorf SA, Rajanayagan V, et al. Resolution improvements in in vivo 1H NMR spectra with increased magnetic field strength. J Magn Reson 1998;135:260–4.

[8] Barker PB, Hearshen DO, Boska MD. Single-voxel proton MRS of the human brain at 1.5 T and 3.0 T. Magn Reson Med 2001;45:765–9.

[9] Gonen O, Gruber S, Li BS, et al. Multi-voxel 3D proton spectroscopy in the brain at 1.5 versus 3.0 T: signal-to-noise ratio and resolution comparison. AJNR Am J Neuroradiol 2001;22:1727–31.

[10] Kantarci K, Reynolds G, Petersen RC, et al. Proton MR spectroscopy in mild cognitive impairment and Alzheimer disease: comparison of 1.5 and 3 T. AJNR Am J Neuroradiol 2003;24:843–9.

[11] Srinivasan R, Vigneron D, Sailasuta N, et al. A comparative study of myo-inositol quantification using LCModel at 1.5 T and 3.0 T with 3 D 1H proton spectroscopic imaging of the human brain. Magn Reson Imaging 2004;22:523–8.

[12] de Graaf RA. In vivo NMR spectroscopy. West Sussex (England): John Wiley & Sons Limited; 1998.

[13] Haacke EM, Brown RW, Thompson MR, et al. Magnetic resonance imaging—physical principles and sequence design. New York (NY): John Wiley & Sons, Incorporated; 1999.

[14] Vlaardingerbroek MT, den Boer JA. Magnetic resonance imaging. New York: Springer-Verlag; 1999.

[15] Bottomley PA, Foster TH, Argersinger RE, et al. A review of normal tissue hydrogen NMR relaxation times and relaxation mechanisms from 1–100 MHz: dependence on tissue type, NMR frequency, temperature, species, excision, and age. Med Phys 1984;11:425–48.

[16] Mlynarik V, Gruber S, Moser E. Proton T (1) and T (2) relaxation times of human brain metabolites at 3 Tesla. NMR Biomed 2001;14:325–31.

[17] Ethofer T, Mader I, Seeger U, et al. Comparison of longitudinal metabolite relaxation times in different regions of the human brain at 1.5 and 3 Tesla. Magn Reson Med 2003;50:1296–301.

[18] Träber F, Block W, Lamerichs R, et al. 1H metabolite relaxation times at 3.0 Tesla: measurements of T1 and T2 values in normal brain and determination of regional differences in transverse relaxation. J Magn Reson Imaging 2004;19: 537–45.

[19] Bottomley PA. Spatial localization in NMR spectroscopy in vivo. Ann N Y Acad Sci 1987;508: 333–48.

[20] Frahm J, Merboldt KD, Hanicke W. Localized proton spectroscopy using stimulated echoes. J Magn Reson 1987;72:502–8.

[21] Hahn EL. Spin Echoes. Phys Rev 1950;80:580–94.

[22] Kim DH, Adalsteinsson E, Glover GH, et al. Regularized higher-order in vivo shimming. Magn Reson Med 2002;48:715–22.

[23] Gruetter R. Automatic, localized in vivo adjustment of all first and second order shim coils. Magn Reson Med 1993;29:804–11.

[24] Provencher SW. Estimation of metabolite concentrations from localized in vivo proton NMR spectra. Magn Reson Med 1993;30:672–9.

[25] Gruber S, Mlynarik V, Moser E. High-resolution 3D proton spectroscopic imaging of the human brain at 3 T: SNR issues and application for anatomy-matched voxel sizes. Magn Reson Med 2003;49:299–306.

[26] Ernst RR, Bodenhausen G, Wokaun A. Principles of nuclear magnetic resonance in one and two dimensions. Oxford (United Kingdom): Clarendon Press; 1987.
[27] Trabesinger AH, Meier D, Boesiger P. In vivo 1H NMR spectroscopy of individual human brain metabolites at moderate field strengths. Magn Reson Imaging 2003;21:1295–302.
[28] Ryner LN, Sorenson JA, Thomas MA. Localized 2D J-resolved 1H MR spectroscopy: strong coupling effects in vitro and in vivo. Magn Reson Imaging 1995;13:853–69.
[29] Thomas MA, Hattori N, Umeda M, et al. Evaluation of two-dimensional L–COSY and JPRESS using a 3 T MRI scanner: from phantoms to human brain in vivo. NMR Biomed 2003;16: 245–51.
[30] Hurd R, Sailasuta N, Srinivasan R, et al. Measurement of brain glutamate using TE-averaged PRESS at 3 T. Magn Reson Med 2004;51:435–40.
[31] Mayer D, Spielman DM. Detection of glutamate in the human brain at 3 T using optimized constant time point resolved spectroscopy. Magn Reson Med 2005;54:439–42.
[32] Schulte RF, Trabesinger AH, Boesiger P. Chemical-shift-selective filter for the in vivo detection of J-coupled metabolites at 3 T. Magn Reson Med 2005;53:275–81.
[33] Kuhn B, Dreher W, Norris DG, et al. Fast proton spectroscopic imaging employing k-space weighting achieved by variable repetition times. Magn Reson Med 1996;35:457–64.
[34] Duyn JH, Moonen CT. Fast proton spectroscopic imaging of human brain using multiple spin echoes. Magn Reson Med 1993;30:409–14.
[35] Haase A, Matthaei D. Spectroscopic FLASH NMR Imaging (SPLASH Imaging). J Magn Reson 1987; 71:550–3.
[36] Park HW, Kim YH, Cho ZH. Fast gradient-echo chemical-shift imaging. Magn Reson Med 1988; 7:340–5.
[37] Guilfoyle DN, Blamire A, Chapman B, et al. PEEP–a rapid chemical-shift imaging method. Magn Reson Med 1989;10:282–7.
[38] Posse S, Tedeschi G, Risinger R, et al. High-speed 1H spectroscopic imaging in human brain by echo planar spatial–spectral encoding. Magn Reson Med 1995;33:34–40.
[39] Norris DG, Dreher W. Fast proton spectroscopic imaging using the sliced k-space method. Magn Reson Med 1993;30:641–5.
[40] Jakob PM, Ziegler A, Doran SJ, et al. Echo time-encoded burst imaging (EBI): a novel technique for spectroscopic imaging. Magn Reson Med 1995; 33:573–8.
[41] Dreher W, Leibfritz D. A new method for fast proton spectroscopic imaging: spectroscopic GRASE. Magn Reson Med 2000;44:668–72.
[42] Adalsteinsson E, Irarrazabal P, Topp S, et al. Volumetric spectroscopic imaging with spiral-based k-space trajectories. Magn Reson Med 1998;39: 889–98.
[43] Tyszka JM, Mamelak AN. Volumetric multi-shot echo–planar spectroscopic imaging. Magn Reson Med 2001;46:219–27.
[44] Adalsteinsson E, Star-Lack J, Meyer CH, et al. Reduced spatial side lobes in chemical-shift imaging. Magn Reson Med 1999;42:314–23.
[45] Kim DH, Margolis D, Xing L, et al. In vivo prostate magnetic resonance spectroscopic imaging using two-dimensional J-resolved PRESS at 3 T. Magn Reson Med 2005;53:1177–82.
[46] Posse S, Otazo R, Caprihan A, et al. Glutamate mapping at 3 and 4 Tesla in human brain using short TE proton echo planar spectroscopic imaging [abstract]. In: Proceedings of the 13th Annual International Society for Magnetic Resonance in Medicine Scientific Meeting. Miami (FL): 2005. p. 2515.
[47] Otazo R, Alger JR, Caprihan A, et al. Quantitative short echo-time spectroscopic imaging at high-field: automated data reconstruction and LCModel fitting [abstract]. In: Proceedings of the 13th Annual International Society for Magnetic Resonance in Medicine Scientific Meeting. Miami (FL): 2005. p. 2460.
[48] Posse S, Xu J, Li T, et al. Large spectral bandwidth with online ramp sampling correction in proton echo planar spectroscopic imaging of human brain at 4 Tesla [abstract]. In: Proceedings of the 13th Annual International Society for Magnetic Resonance in Medicine Scientific Meeting. Miami (FL): 2005. p. 2513.
[49] Gu M, Kim DH, Adalsteinsson E, et al. Brain 3D MRSI using dual-band spectral–spatial excitation and k-space corrected spiral readout [abstract]. In: Proceedings of the 13th Annual International Society for Magnetic Resonance in Medicine Scientific Meeting. Miami (FL): 2005. p. 2763.
[50] Chen AP, Cunningham CH, Xu D, et al. High-speed MR spectroscopic imaging of cancer using flyback echo–planar encoding [abstract]. In: Proceedings of the 13th Annual International Society for Magnetic Resonance in Medicine Scientific Meeting. Miami (FL): 2005. p. 2062.
[51] Pruessmann KP, Weiger M, Scheidegger MB, et al. SENSE: sensitivity encoding for fast MRI. Magn Reson Med 1999;42:952–62.
[52] Jaermann T, Crelier G, Pruessmann KP, et al. SENSE-DTI at 3 T. Magn Reson Med 2004;51: 230–6.
[53] Dydak U, Weiger M, Pruessmann KP, et al. Sensitivity-encoded spectroscopic imaging. Magn Reson Med 2001;46:713–22.
[54] Lin FH, Caprihan A, Wald LL, et al. Sensitivity-encoded proton echo planar spectroscopic imaging (PEPSI) of human brain [abstract]. In: Proceedings of the 13th Annual International Society for Magnetic Resonance in Medicine Scientific Meeting. Miami (FL): 2005. p. 489.
[55] Dydak U, Pruessmann KP, Weiger M, et al. Parallel spectroscopic imaging with spin-echo trains. Magn Reson Med 2003;50:196–200.
[56] Duyn JH, Frank JA, Moonen CT. Incorporation

of lactate measurement in multi-spin echo proton spectroscopic imaging. Magn Reson Med 1995;33:101–7.
[57] Flacke S, Träber F, Block W, et al. Improved diagnosis of contrast-enhancing brain lesions with multifunctional MRI assessment: a case report. J Magn Reson Imaging 1999;9:741–4.
[58] Martin AJ, Liu H, Hall WA, et al. Preliminary assessment of turbo spectroscopic imaging for targeting in brain biopsy. AJNR Am J Neuroradiol 2001;22:959–68.
[59] Träber F, Block W, Flacke S, et al. 1H-MR Spectroscopy of brain tumors in the course of radiation therapy: use of fast spectroscopic imaging and single-voxel spectroscopy for diagnosing recurrence. Rofo 2002;174:33–42.
[60] Block W, Jessen F, Träber F, et al. Regional N-acetylaspartate reduction in the hippocampus detected with fast proton magnetic resonance spectroscopic imaging in patients with Alzheimer's disease. Arch Neurol 2002;59:828–34.
[61] Dydak U, Meier D, Lamerichs R, et al. High-resolution MRSI in less than a minute. In abstract of the 20th Annual Scientific Meeting ESMRMB; September 18–21, 2003; Rotterdam, The Netherlands. Abstract 41.
[62] Nelson SJ, Vigneron DB, Star-Lack J, et al. High spatial resolution and speed in MRSI. NMR Biomed 1997;10:411–22.
[63] Tran TK, Vigneron DB, Sailasuta N, et al. Very selective suppression pulses for clinical MRSI studies of brain and prostate cancer. Magn Reson Med 2000;43:23–33.
[64] Conolly S, Glover G, Nishimura D, et al. A reduced power selective adiabatic spin echo pulse sequence. Magn Reson Med 1991;18:28–38.
[65] Slotboom J, Mehlkopf AF, Bovee WMMJ. A single-shot localization pulse sequence suited for coils with inhomogeneous RF fields using adiabatic slice-selective RF pulses. J Magn Reson 1991;95:396–404.
[66] Garwood M, DelaBarre L. The return of the frequency sweep: designing adiabatic pulses for contemporary NMR. J Magn Reson 2001;153:155–77.
[67] Danielsen ER, Ross B. Magnetic resonance spectroscopy diagnosis of neurological diseases. New York, NY: Marcel Dekker Limited; 1999.
[68] Yablonskiy DA, Neil JJ, Raichle ME, et al. Homonuclear J coupling effects in volume localized NMR spectroscopy: pitfalls and solutions. Magn Reson Med 1998;39:169–78.
[69] Kelley DA, Wald LL, Star-Lack JM. Lactate detection at 3T: compensating J coupling effects with BASING. J Magn Reson Imaging 1999;9:732–7.
[70] Lange T, Dydak U, Roberts TPL. Pitfalls in lactate measurements at 3 T. AJNR Am J Neuroradiol 2006;27(4):892–8.